Nanoscale

Accepted Manuscript

This article can be cited before page numbers have been issued, to do this please use: Z. Guan and S. Ni, *Nanoscale*, 2020, DOI: 10.1039/D0NR04837B.

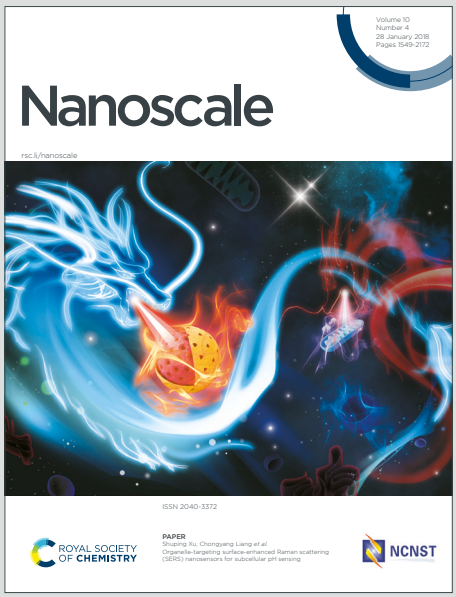

ROYAL SOCIETY OF CHEMISTRY

rsc.li/nanoscale

View Article Online
DOI: 10.1039/D0NR04837B

Prediction 2D Ferromagnetic Janus VSeTe Monolayer with High Curie Temperature, Large Valley Polarization and Magnetic Crystal Anisotropy

Zhaoyong Guan,[†§*] *Shuang Ni*[ξ]

[†]Key Laboratory of Colloid and Interface Chemistry, Ministry of Education, School of Chemistry and Chemical Engineering, Shandong University, Jinan, Shandong 250100, P. R. China

[§]Scientific Research Center for Material Creation and Energy Conversion, Shandong University, Qingdao, Shandong 266237, P. R. China

[ξ] Research Center of Laser Fusion, China Academy of Engineering Physics. Mianyang, Sichuan 621900, P. R. China

View Article Online
DOI: 10.1039/D0NR04837B

ABSTRACT

Two-dimensional (2D) intrinsic ferromagnetic semiconductors are urgent in the spintronic field. Motivated by the recent experiments on the successful synthetization of monolayer (ML) Janus transition-metal dichalcogenides (MoSSe) and ferromagnetic (FM) VSe_2, a highly stable ML Janus 2H-VSeTe is fabricated by density functional theory and confirmed by a global minimum search. The Janus VSeTe shows a large valley polarization of 158 meV as the space- and time-reversal symmetry broken. The VSeTe shows FM order with Curie temperature (T_c) of 350 K, and sizable magnetocrystalline anisotropy (MCA) of -8.54 erg/cm^2. The high T_c and large valley polarization imply 2D Janus VSeTe as a promising magnetic material for potential applications in electronics, spintronics, and valleytronics.

Keywords: Janus VSeTe, valley, ferromagnetic, Curie temperature, magnetocrystalline anisotropy

1. INTRODUCTION

View Article Online
DOI: 10.1039/D0NR04837B

2D materials, such as graphene,[1-4] transition metal dichalcogenides (MoS_2),[5-6] hexagonal boron nitride,[7] stanene,[8] CrI_3[9] show novel properties in electronics[8, 10-12] and spintronics.[13-15] It is well known that long-range magnetic orders at finite temperature in a 2D system is prohibited by the strong fluctuations, as depicted by the Mermin–Wagner theorem.[16] Therefore, 2D magnetic materials for spintronics appear until recent years. [17] However, they are limited in two aspects.[13, 18] One aspect is the materials have ferromagnetic (FM) order with semiconducting properties are rare.[18] Another aspect is T_c of intrinsic ferromagnetic materials are usually much lower than the room temperature.[9, 17] To overcome the limitations, researchers try to modulate,[19-20] synthesize[9, 17] and design[11-12, 14, 21-22] novel and stable magnetic semiconductors.[23-24] As important members of 2D ferromagnetic semiconductors, CrI_3,[7] $Cr_2Ge_2Te_6$[13] and VSe_2[25] have attracted much attention for their intrinsic ferromagnetism.[26] Morever, people also focus on the materials with various spin configurations,[27] different electronic properties,[3] and higher magnetic anisotropy energy (MAE)[28-29] in the development of 2D magnetic devices. As the MoSSe is successfully synthetized, [30] it is expected that Janus

View Article Online
DOI: 10.1039/D0NR04837B

structures are newly developed 2D materials with intriguing physical properties.[31] The successfully synthesized 2D Janus materials could work as field-effect transistors,[30] ultra-sensitive detectors,[31] spintronic,[18, 32] and valleytronic devices.[33] Janus MoSSe [34] and $GaInX_2$ (X=S, Se, Te)[35] present strong piezoelectric effect. TiSO[36] and MoSSe[37] have appropriate optical redox potentials for photocatalyst. Intrinsic ferromagnetism[32] and Rashba-type spin splitting[38] are predicted in $Cr_2I_3Cl_3$. Morever, Magnetic skyrmions have been observed in MnSTe (MnSeTe, MnSSe)[4] and MoSSe.[38]

On the other hand, the experimental realization of 2D magnets,[24, 39-43] especial VSe_2,[44]may provide an exciting new platform for the spintronics. VSe_2 is composed of three atomic layers like sandwich,[44] which provides a platform of Janus structure with intrinsic magnetism.[21] Morever, both ML VSe_2[25, 44] and VTe_2[3] are intrinsic ferromagnetic semiconductors. Thus, the time symmetry has been broken in VX_2 (X = Se, Te). Janus VSeTe also breaks mirror and time symmetry, which would introduce new physical phenomena.[31, 34-35, 45-46] A deep understanding of intrinsic physical properties of Janus structures and investigation of the potential applications is highly required.

View Article Online
DOI: 10.1039/D0NR04837B

2. COMPUTATIONAL DETAILS

The geometry search for 2D Janus VSeTe has been carried out by using the PSO method implemented in the CALYPSO code.[47] The calculations of the Janus VSeTe properties are performed by using the plane-wave basis Vienna Ab initio Simulation Package (VASP) code,[48-49] based on the density functional theory under the generalized gradient approximation (GGA) with Perdew-Burke-Ernzerhof (PBE).[50] The strong-correlated correction is considered with GGA+U[51] method to deal with the V's 3*d* electrons. The effective onsite Coulomb interaction parameter (*U*) and exchange interaction parameter (*J*) are set to be 2.00 and 0.84 eV for V's 3*d* electrons. The effective *U*-*J* is set 1.16 eV, following the routines.[3, 21] And some key issues are confirmed by HSE06.[52-53] The vacuum space in the *z*-direction is set 16 Å to avoid the virtual interactions. The kinetic energy cutoff is set as 400 eV. And the geometries are fully relaxed until energy and force is converged to 10^{-6} eV and 1 meV/Å, respectively. Monkhorst-Pack[54] of *k*-grids with 16×16×1, 26×26×1, and 36×36×1 are adopted in Brillouin zone integration for geometry optimization, energy and density of states (DOS)

View Article Online
DOI: 10.1039/D0NR04837B

computation, respectively. And 240 uniform k-points along high-symmetry special *k*-paths are used to obtain band structure. The MCA is calculated with an energy cutoff of 400 eV and convergence of 1×10^{-8} eV for total energy. And the corresponding *k*-grid is adopted 66×66×1, with non-symmetric constriction. The details of convergence test on MCA are shown in Figure S1, Supporting Information. The phonon spectra and density of states are calculated using finite displacement method as implemented in the Phonopy software,[55] and a 6×6×1 cell is used in calculation. The criterion critical for the total energy and the Hellmann-Feynman force is 10^{-8} eV and 1 meV/Å in phonon spectra calculation, respectively. 2000 uniform *k*-points along high-symmetry lines are used to obtain the phonon spectra. *Ab initio* molecular dynamics (AIMD) simulation is also performed. The constant moles–volume–temperature (NVT) ensemble with Nosé–Hoover thermostat[56] is adopted at temperature of 300 K. And the time step and total time are 1 fs and 10 ps, respectively. In order to eliminate effect of the periodic boundary condition in AIMD simulation with relatively smaller system size, which can artificially increase the stability of the structures. A larger supercell (2×2×1 cell) is adopted in the AIMD simulation.

View Article Online
DOI: 10.1039/D0NR04837B

3. RESULTS AND DISCUSSION

3.1. Geometry of ML Janus VSeTe. The geometries of ML Janus 2H-VSeTe (with VSeTe in short) and T-VSeTe are fabricated, and confirmed by particle swarm optimization (PSO) based on the crystal structure analysis, shown in Figure 1a-b and S2. The corresponding optimized lattice parameter of H-VSeTe is $a = b = 3.486$ Å. We use two different methods to optimize the geometry. We have fit the energies versus the lattice parameters, and gotten the optimized lattice parameter, which is the same with lattice with global optimization. From the optimized geometry, we can find that ML Janus VSeTe presents C_{3v} point group, different from D_{3d} of VTe_2 and VSe_2. The Janus VSeTe breaks the out-of-plane structure symmetry, as the two sides are positioned Se and Te atoms, respectively. And both FM and antiferromagnetic (AFM) orders are considered, shown in Figure 1c-d, respectively. The geometries with different orders have the same optimized lattice. The corresponding V-Se and V-Te bonds are 2.728 and 2.514 Å, respectively. And these values are the same with VTe_2 (2.727 Å) and VSe_2 (2.512 Å),[25] respectively. The vertical distance between Se and V atoms, and Te are V atoms are

View Article Online
DOI: 10.1039/D0NR04837B

1.507 and 1.840 Å, respectively. There is 0.68 *e* electron transferring from V atom to Te (0.28 *e*), and Se (0.40 *e*) atoms, respectively. Compared with Te atoms, Se atoms get more electrons for the latter's stronger electronegativity. Each V atoms contributes 1.22 μ_B magnetic moment, and the supercell has 1.0 μ_B. There is 4.0 μ_B in the supercell (2×2×1 cell) for the FM order. While each two V atoms has 1.04 μ_B magnetic moment, and the other two V atoms have -1.04 μ_B magnetic moment for the AFM order. Therefore, the total magnetic moment equals to 0 μ_B. The corresponding energy difference is defined as $\Delta E = E_{AFM} - E_{FM} = 0.523$ eV, so the ML Janus VSeTe is an intrinsic ferromagnetic material. The geometrical and electronic properties of T-VSeTe are shown in the Figure S2, in the Supporting Information. And T-VSeTe shows AFM

View Article Online
DOI: 10.1039/D0NR04837B

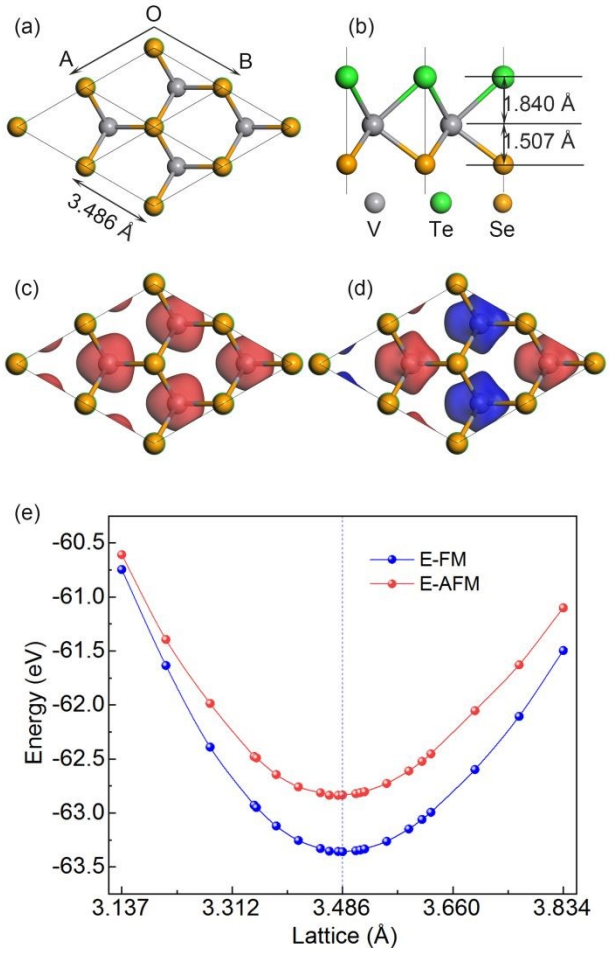

Figure 1. (a) Top and (b) side views of the optimized geometry of ML Janus 2H-VSeTe. The grey, green, and yellow balls represent V, Te, and Se atoms, respectively. (c-d) Spin charge densities of (c) FM and (d) AFM of VSeTe. The isovalue is 0.06 e/Å^3. (e) The energies of FM and AFM orders are fitted versus the lattice. The blue and red lines present energies of FM and AFM orders, respectively.

ground states, and more details could be found in Supporting Information.

View Article Online
DOI: 10.1039/D0NR04837B

3.2. Electronic Structure. In the above section, the geometry of 2H-VSeTe is discussed, while the electronic properties are still unknown. The electronic properties are systematically investigated in this section. The valance band maximum (VBM) occupied by the spin-α electron, is located at Γ point of the Brillouin zone (BZ). While the conduction band minimum (CBM) contributed by spin-β electrons, is located at K (K`) point of the BZ. Therefore, ML Janus VSeTe is a bipolar magnetic semiconductor (BMS), with an indirect band gap of 0.254 eV. And this issue is also confirmed by Heyd-Scuseria-Ernzerhof (HSE06) functional, shown in Figure S3, Supporting Information. As BMSs, the gaps of spin-α ($E_{g\text{-}\alpha}$) and spin-β ($E_{g\text{-}\beta}$) channels are usually different. For the spin-α channel electrons, the VBM is located at Γ point, while the CBM is located at K point. And the corresponding $E_{g\text{-}\alpha}$ equals to 0.342 eV. For the spin-β electrons, the VBM is located at Γ point, while the CBM is located at M point. And the corresponding $E_{g\text{-}\beta}$ is 0.481 eV. Both VBM and CBM are mainly contributed by V atom, shown in Figure 1d-g. From the analysis of the partial density of the states (DOS), the VBM is mainly consisted of d_{xz} and d_{yz} orbitals of V atom, shown in Figure S4,

View Article Online
DOI: 10.1039/D0NR04837B

Supporting Information. And this point is also confirmed by the charge densities, shown in Figure 2d-e. However, the CBM is mainly contributed by the d_{z^2} orbital of V atom, which is shown in Figure 2f-g.

3.3. Valley. The V element is heavy element, so the spin-orbital coupling (SOC) should be considered in the simulation. And this would reduce the degeneracy of the band structure of certain k-points of high symmetry.[8] The spin-resolved band structures obtained with SOC is presented in Figure 2h. The gaps at K and K` points of the BZ are 659 and 501 meV, respectively. Most interestingly, a local minimum in the conduction band (CB) and a local maximum in the valence band (VB) is referred to as valley, shown in Figure 2h. More details could be found in Figure S5, Supporting Information. A large valley polarization of 158 meV is achieved in VSeTe, which is large enough to observe the valley Hall effect at room temperature. The induced valley polarization is larger than VSSe (85 meV),[21] Cr doped MoSSe (59 meV),[33] WSe_2 with defects (1 meV),[57] WSe_2 under an magnetic field (0.2 meV),[58] and MoS_2 under an electric field (3 meV).[59] Morever, it is unnecessary to use electron or hole dope, defects, high magnetic

View Article Online
DOI: 10.1039/D0NR04837B

and electric fields, which are not easy to control in the experiment to achieve valley polarization.[60] Therefore, Janus VSeTe could be interesting for quantum information processing using valley freedom.

The valley polarization contributed by the vanadium $d_{x^2-y^2}$, d_{z^2} and d_{xy} orbitals, is mainly located at K and K` points, shown in Figure S6, Supporting Information. It is predicted to be caused by the combination of SOC and exchange interaction.[21] Compared with H-VSSe, the H-VSeTe has much stronger SOC effect as the latter has heavier element-Te. [21] The strong SOC enhances the spin splitting of 158 meV at K`/K valleys, which is larger than VSSe. The corresponding three-dimensional (3D) plots of VB and CB is also shown in Figure 2i. The energies of VB at K and K` points are not the global but the localized maximum point, while it is the global minimum point (CBM), shown in Figure 2i. And Figure S5 in Supporting Information could provide more details.

View Article Online
DOI: 10.1039/D0NR04837B

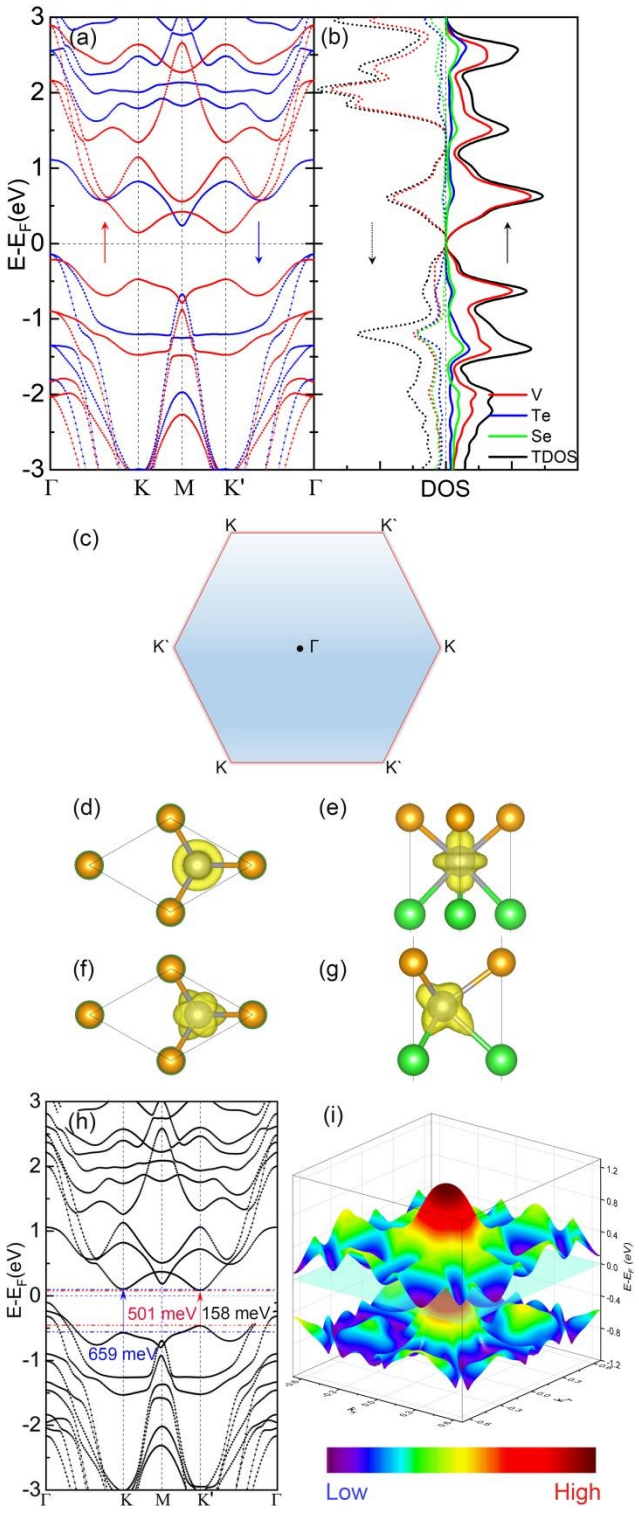

Figure 2. (a) Band structure of ML Janus VSeTe. The red and blue present spin-α and spin-β electrons, respectively. (b) DOS of ML VSeTe. And the red, blue, and green dots

View Article Online
DOI: 10.1039/D0NR04837B

present projected DOS from the V, Te, and Se atoms, respectively. (c) The K and K` points are shown in the first BZ. (d-g) Charge densities of the ML MoSSe: (d) Top and (e) side views of wavefunction of VBM and (e, f) of CBM, respectively. And the isovalue is 0.02 e/ Å$^3$. The Γ, M, K, K` *k*-points are (0, 0, 0), (0, 1/2, 0), (-1/3, 2/3, 0), and (1/3, 1/3, 0), respectively. (h) The band structure of ML Janus VSeTe with SOC along magnetization axis [001]. The blue, red and black figures show the gap at K, K` kpoints and valley splitting. (i) 3D plots of VB and CB. The different colors show different iso-surfaces.

3.4. Currie Temperature

The ferromagnetic materials, especial high Curie temperature (T_c) materials are highly desirable. It is expected that T_c should be comparable to the room temperature (300 K) in the actual applications. We use classic Heisenberg model to evaluate the magnetic exchange parameters (*J*). The considered magnetic configurations are shown in Figure 3, assuming nearest neighbor interactions only. And the Hamiltonian can be written as:

View Article Online
DOI: 10.1039/D0NR04837B

$$H = -J\sum_{<i,j>} S_i * S_j \quad (1)$$

$$E_{FM} = E_0 - (\frac{1}{2}\times 6\times 4)J|S|^2 \quad (2)$$

$$E_{AFM} = E_0 + 4\times(-\frac{1}{2}\times 2 + \frac{1}{2}\times 4)J|S|^2 \quad (3)$$

$$J = \frac{E_{AFM} - E_{FM}}{16|S|^2} \quad (4)$$

Where E_{FM} and E_{AFM} present energies of FM and AFM orders, respectively. *J* and *H* are the exchange parameter and Hamilton, respectively, and S_i presents the spin operator. Each V atom contributes 1.00 μ_B magnetic moment. The magnetic energies of the 2×2×1 supercell with FM and AFM orders could be calculated by eqs 2-3, respectively. The corresponding exchange parameter is evaluated with eq 4. The calculated exchanged parameter is $J = 32.81\, meV$. Considering the disadvantage of the mean field theory, we use classic Heisenberg model Monte Carlo (MC) simulations[61] to evaluate the magnetic moment as a function of temperature to calculate T_c. And the corresponding MC code is developed by Prof. Hongjun Xiang's group. [61] Using this method, the estimated T_c of CrI_3 is about 51 K, which is in agreement the experimental measurement of 45 K.[9] 1.0×10[6] loops with an 80×80 supercell is adopted in the T_c

View Article Online
DOI: 10.1039/D0NR04837B

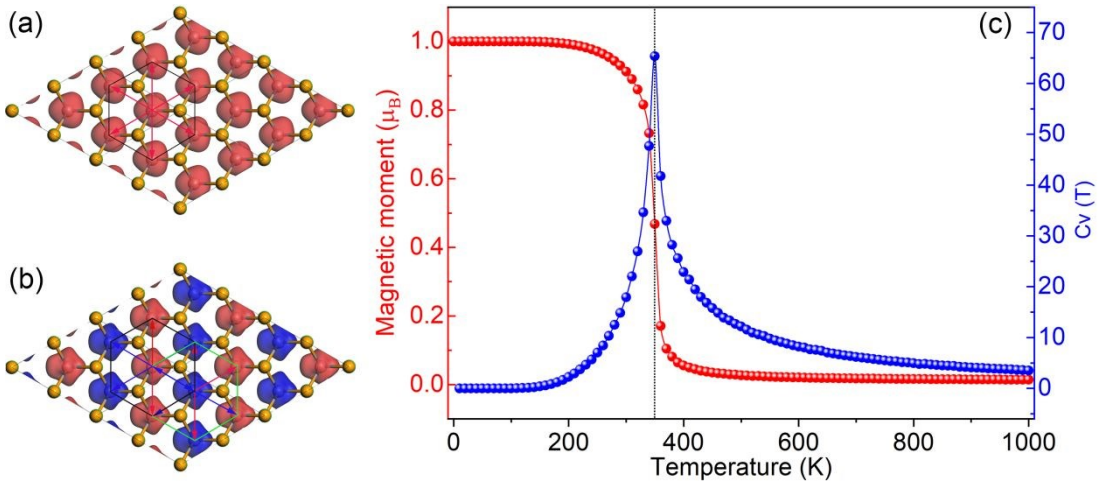

Figure 3. (a-b) Heisenberg model considering the nearest exchange interactions. The spin densities of (a) FM and (b) AFM orders of Janus VSeTe. The red and blue colors present spin-α and spin-β electron densities, respectively. The red and blue arrows present V atom ferromagnetically and antiferromagnetically coupling with the nearest V atoms, respectively. (c) The magnetic moment per unit cell (red) and specific heat (C_v) (blue) vary with respect to temperature from classic Heisenberg model Monte Carlo (MC) simulation.

calculation. In the simulation, the spins on all the magnetic sites flip randomly. We also test the effect of larger supercells and longer loops on T_c, and they show the similar results. The total magnetic moment per unit cell starts dropping gradually from 1.00 μ_B

View Article Online
DOI: 10.1039/D0NR04837B

at about 200 K, and the paramagnetic order is achieved at a temperature of 400 K for Janus VSeTe, shown in Figure 3c. The corresponding T_c is predicted to be 350 K, which is higher than the room temperature (300 K). It indicates that the intrinsic ferromagnetic can persist above room temperature.

3.5. Magnetocrystalline Anisotropy

When a magnetic moment is switched from the easy axis (EA) to the hard axis will cost MAE. The MCA is defined as the MAE of the per area, and evaluated with eqs 5 and 6.

$$MAE = E_{[100]} - E_{[001]} \quad (5)$$

$$MCA = E_{[100]} - E_{[001]} = MAE / S \quad (6)$$

Where $E_{[100]}$ and $E_{[001]}$ present energy along [100] and [001] direction, and S presents the area of unit cell. MCA is an important parameter for magnetic materials, which determines the orientation of EA. Reduced dimensionality and broken symmetry would increase MCA several orders of magnitude larger than that of conventional bulk systems.[62] Janus VSeTe is 2D structure, which is expected a sizable MCA. The MCA could be evaluated with DFT calculations with SOC. In order to determine the EA, three

View Article Online
DOI: 10.1039/D0NR04837B

magnetization directions, that is, [100], [010], and [001] are investigated. The energy difference along different directions is $MAE = -2.80\ \mathrm{meV/(V\ atom)}$, which implies the EA is long [100] direction, shown in Figure 4a. The corresponding MCA of Janus VSeTe is -8.54 erg/cm^2. Why the EA of VSeTe is along [100] direction? We try to explain the reason from the orbital-resolved band structures with SOC.

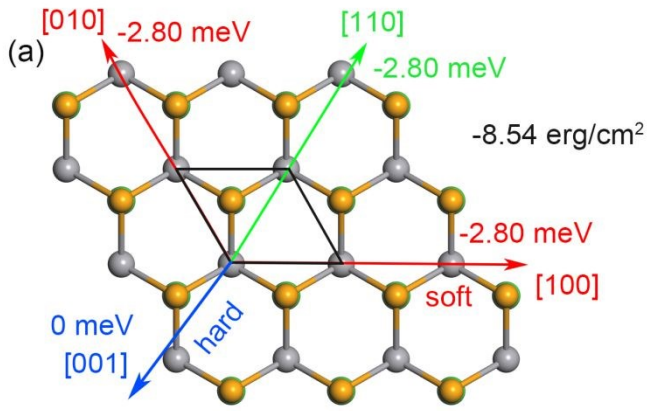

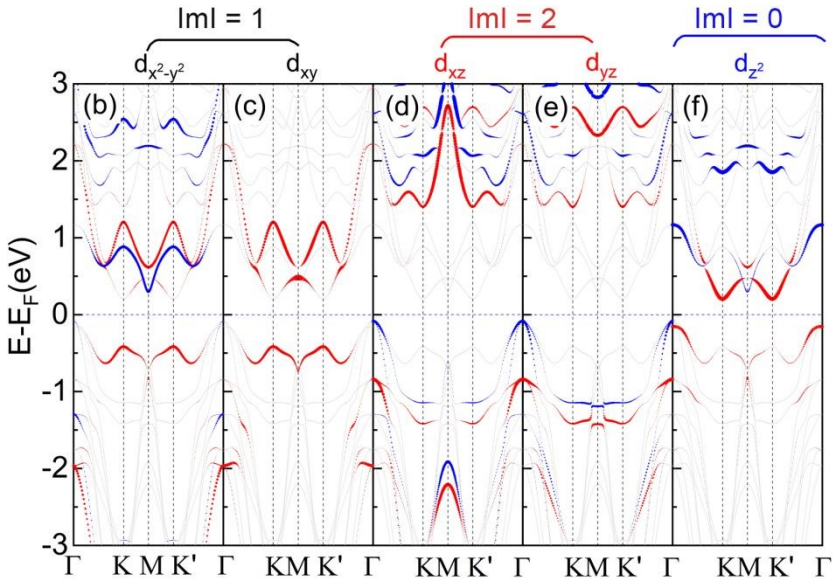

View Article Online
DOI: 10.1039/D0NR04837B

Figure 4. (a) The optimized structure of Janus VSeTe. The figures present the MAE and MAC with respect to the perpendicular axis ([001] direction). The different arrows correspond to the different axes. (b) The projected band structure with (b) $d_{x^2-y^2}$, (c) d_{xy}, (d) d_{xz}, (e) d_{yz}, and (f) d_{z^2} orbitals of V atom, respectively. The fermi level is set to 0.

In 1993, Prof. Wang proposed that MCA could be expressed using second-order perturbation theory[63]:

$$\mathrm{MCA} = \xi^2 \sum_{o,u} \frac{\left|\langle \Psi_o^{\uparrow(\downarrow)} \left| \hat{L}_z \right| \Psi_u^{\uparrow(\downarrow)} \rangle\right|^2 - \left|\langle \Psi_o^{\uparrow(\downarrow)} \left| \hat{L}_x \right| \Psi_u^{\uparrow(\downarrow)} \rangle\right|^2}{E_u^{\uparrow(\downarrow)} - E_o^{\uparrow(\downarrow)}} + \underbrace{\frac{\left|\langle \Psi_o^{\uparrow(\downarrow)} \left| \hat{L}_x \right| \Psi_u^{\uparrow(\downarrow)} \rangle\right|^2 - \left|\langle \Psi_o^{\uparrow(\downarrow)} \left| \hat{L}_z \right| \Psi_u^{\uparrow(\downarrow)} \rangle\right|^2}{E_u^{\uparrow(\downarrow)} - E_o^{\uparrow(\downarrow)}}}_{\text{spin-flip term}} \quad (7)$$

Where $\Psi_o^{\uparrow}(E_o^{\downarrow})$ and $\Psi_u^{\uparrow}(E_u^{\downarrow})$ are the one-electron occupied and unoccupied spin-β states of band *n* and wave vector *k*. ξ is the SOC constant, and $\hat{L}_{z(x)}$ is the *z (x)* component of the orbital angular momentum operator. For the electrons with the same spin, the MCA positively contributed by the same magnetic quantum number are divided into two parts: $\left\langle x^2 - y^2 \left| \hat{L}_z \right| xy \right\rangle$ and $\left\langle xz \left| \hat{L}_z \right| yz \right\rangle$. While the MCA negatively contributed

View Article Online
DOI: 10.1039/D0NR04837B

by the different magnetic quantum numbers are divided into three parts: $\left\langle xy\left|\hat{L}_x\right|xz\right\rangle\left(\left|yz\right\rangle\right)$, $\left\langle z^2\left|\hat{L}_x\right|xz\right\rangle\left(\left|yz\right\rangle\right)$, and $\left\langle x^2-y^2\left|\hat{L}_x\right|xz\right\rangle\left(\left|yz\right\rangle\right)$. SOC between different spin states gives a reverse contribution to MCA.

In order to simplify the problem, people usually consider the contribution form the states near the fermi-level. In other word, only the effect of the VBM, CBM and nearby CBs on the MCA is taken into consideration. The VBM are mainly contributed by vanadium d_{xz} and d_{yz} orbitals occupied by spin-β electrons. While the CBM and nearby CBs are contributed by vanadium d_{z^2} orbital of spin-α electrons, $d_{x^2\text{-}y^2}$ and d_{z^2} orbitals of spin-β electrons, respectively. From the above analysis, the in-plane MCA mainly comes from the positive contribution of $\left\langle z^2\left|\hat{L}_x\right|xz\right\rangle\left(\left|yz\right\rangle\right)$, and the negative contribution of $\left\langle x^2-y^2\left|\hat{L}_x\right|xz\right\rangle\left(\left|yz\right\rangle\right)$ with different magnetic quantum numbers. There is a competition between two opposite parts. As a result, the MCA is negative, implying EA is along in-plane axis ([100] direction).

View Article Online
DOI: 10.1039/D0NR04837B

3.6. The dynamical and thermal stability. The dynamical stability of ML Janus VSeTe is confirmed via phonon dispersion curves and phonon density of the states, which show no obvious imaginary phonon modes. The imaginary phonon modes could be ignored compared with the highest vibration frequency. The highest vibration frequency is 9.65THZ, which is higher than ML VTe_2 (8.73 THZ), but smaller than VSe_2 (9.83 THZ), shown in Figure S7, Supporting Information. And it is relative with the mechanical robustness of the covalent bonds. From the Figure 5b, we can find that the contribution mainly comes from Se and Te atoms for the low frequency ($0 < \varepsilon < 5$ THZ). On the contrary, V atoms make the main contribution, for the high frequency ($7 < \varepsilon < 10$ THZ). And this may affect the thermal properties of the VSeTe. Compared Se (atomic weight: 78.96)/Te (127.6) atoms, the V (50.94) atom is lighter. Therefore, the V atom makes contribution to the phonon with high energy, while the Se/Te atoms make contribution to the phonon with low energy, shown in Figure 5 (b). At low temperature, the thermal conductivity is mainly contributed by the phonon with low-frequency (Se/Te atoms). However, the thermal conductivity is mainly contributed by the phonon with high-frequency (V atom), at high temperature.

View Article Online
DOI: 10.1039/D0NR04837B

The thermal stability of Janus VSeTe is also evaluated with the AIMD, which is widely used to investigate the geometrical properties of 2D materials. To examine whether Janus VSeTe is stable and the magnetic order could survive at room temperature, we also perform AIMD simulations at 300 K. The fluctuations in the total energies are shown in Figure 5, c. The total energies vibrate round -62.800 eV at 300 K, with the amplitude about 0.035 eV per atom. And the snapshots of the geometries also confirm the essential intact sandwich-like structures. No obvious structure destruction is found, and Janus VSeTe is expected to stabilize at 300 K. Morever, the evaluation of magnetic moment changes with the temperature is also investigated. The total magnetic moment is about 4.0 μ_B in simulated time. It is sure that Janus VSeTe presents ferromagnetic ground, and geometries are stable at room temperature.

View Article Online
DOI: 10.1039/D0NR04837B

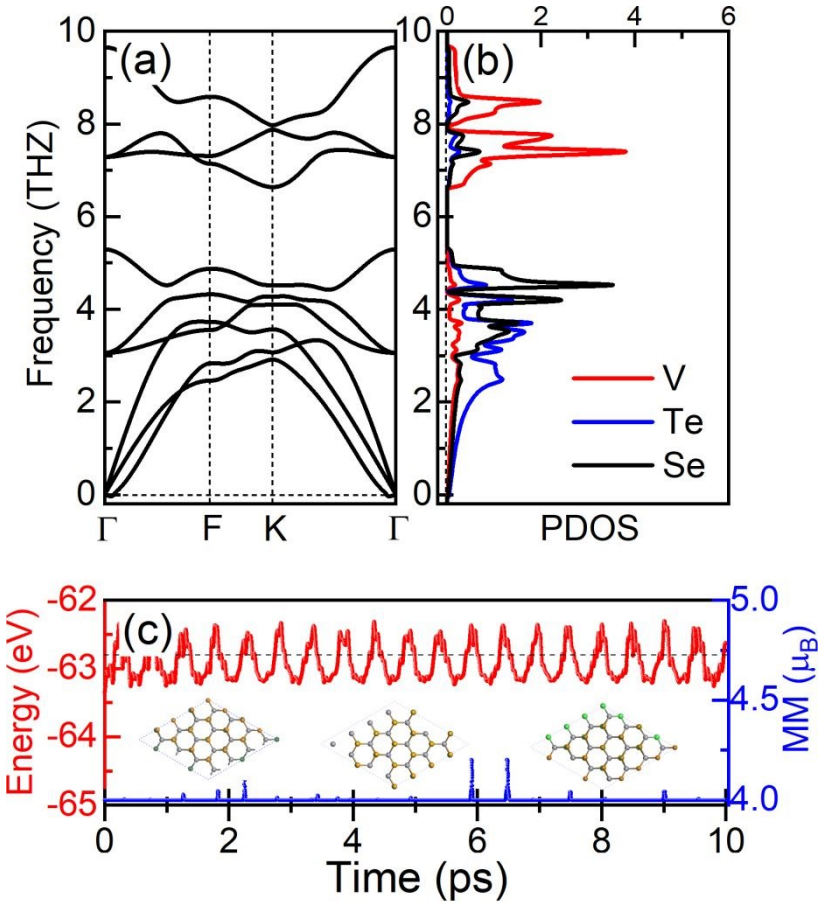

Figure 5. (a) The phonon spectrum and (b) phonon density of the state of the ML Janus VSeTe. The red, blue, and black lines present V, Te and Se atoms projected phonon DOS, respectively. (c) AIMD of the evaluation of energy at PBE+U level for 10 ps at 300 K. The red and blue lines present total energies and magnetic moment, respectively. The inset are the atomic structure snapshots at some time from AIMD.

3. CONCLUSIONS

View Article Online
DOI: 10.1039/D0NR04837B

In conclusion, we have predicted a new intrinsic ferromagnetic ML Janus VSeTe. We have found ferromagnetism in ML Janus H-VSeTe, by using particle-swarm search approaches and first-principles. A Curie temperature above room temperature makes VSeTe potentially attractive material. The obvious valley polarization can be realized by SOC in VSeTe. The EA is along [100] direction, and the corresponding MCA is also sizable, insuring the magnetic stability. The phonon spectrum and AIMD confirm the stability of Janus VSeTe. Our work presents ferromagnetic and valley-polarized Janus VSeTe with high Curie temperature, implying its potential application in spin-electronics, optoelectronics, and valleytronics.

Supporting Information

Information on materials, MAE change with *k*-mesh, geometry and electronic properties of T-VSeTe, band structure and DOS of H-VSeTe with HSE06, PDOS of T-VSeTe, 2D plots CB and VB with SOC, *d*-orbital projected-band structure with SOC, phonon spectrum and density of the states (calculated by PBE) of VSe_2 and VTe_2, synthetization of VSeTe, parameters in Calypso.

View Article Online
DOI: 10.1039/D0NR04837B

Author Information

Corresponding Author

*E-mail: zyguan@sdu.edu.cn; Tel: +86-0531-88363179; Fax: +86-0531-88363179

Acknowledgements

We thank Prof. Xingxing Li for discussion of evaluation of the Currie temperature. We thank doctor Xuelei Sui and Yang Li for discussion of MCA and phonon spectrum calculation. We thank Prof. Zhifeng Liu for calculation of 2D band structure. This work was supported by the financial support from the Natural Science Foundation of China (Grant No. 11904203), the Fundamental Research Funds of Shandong University (Grant No. 2019GN065). The computational resources from Shanghai Supercomputer Center, and National supercomputing Center of Guangzhou should be acknowledged.

Conflict of Interest: The authors declare no competing financial interest.

REFERENCES

(1) Novoselov, K. S.; Geim, A. K.; Morozov, S. V.; Jiang, D.; Zhang, Y.; Dubonos, S. V.; Grigorieva, I. V.; Firsov, A. A. Electric field effect in atomically thin carbon films. *Science* **2004,** *306* (5696), 666-669, DOI: 10.1126/science.1102896.

View Article Online
DOI: 10.1039/D0NR04837B

(2) Stankovich, S.; Dikin, D. A.; Dommett, G. H. B.; Kohlhaas, K. M.; Zimney, E. J.; Stach, E. A.; Piner, R. D.; Nguyen, S. T.; Ruoff, R. S. Graphene-based composite materials. *Nature* **2006,** *442* (7100), 282-286, DOI: 10.1038/nature04969.

(3) Fuh, H.-R.; Chang, C.-R.; Wang, Y.-K.; Evans, R. F. L.; Chantrell, R. W.; Jeng, H.-T. Newtype single-layer magnetic semiconductor in transition-metal dichalcogenides VX2 (X=S, Se and Te). *Sci. Rep.* **2016,** *6* (1), 32625, DOI: 10.1038/srep32625.

(4) Yuan, J.; Yang, Y.; Cai, Y.; Wu, Y.; Chen, Y.; Yan, X.; Shen, L. Intrinsic skyrmions in monolayer Janus magnets. *Phys. Rev. B* **2020,** *101* (9), 094420, DOI: 10.1103/PhysRevB.101.094420.

(5) Coleman, J. N.; Lotya, M.; O'Neill, A.; Bergin, S. D.; King, P. J.; Khan, U.; Young, K.; Gaucher, A.; De, S.; Smith, R. J.; Shvets, I. V.; Arora, S. K.; Stanton, G.; Kim, H.-Y.; Lee, K.; Kim, G. T.; Duesberg, G. S.; Hallam, T.; Boland, J. J.; Wang, J. J.; Donegan, J. F.; Grunlan, J. C.; Moriarty, G.; Shmeliov, A.; Nicholls, R. J.; Perkins, J. M.; Grieveson, E. M.; Theuwissen, K.; McComb, D. W.; Nellist, P. D.; Nicolosi, V. Two-Dimensional Nanosheets Produced by Liquid Exfoliation of Layered Materials. *Science* **2011,** *331* (6017), 568-571, DOI: 10.1126/science.1194975.

(6) Wang, Q. H.; Kalantar-Zadeh, K.; Kis, A.; Coleman, J. N.; Strano, M. S. Electronics and optoelectronics of two-dimensional transition metal dichalcogenides. *Nat. Nanotech.* **2012,** *7* (11), 699-712, DOI: 10.1038/nnano.2012.193.

(7) Golberg, D.; Bando, Y.; Huang, Y.; Terao, T.; Mitome, M.; Tang, C.; Zhi, C. Boron Nitride Nanotubes and Nanosheets. *ACS Nano* **2010,** *4* (6), 2979-2993, DOI: 10.1021/nn1006495.

(8) Liao, M.; Zang, Y.; Guan, Z.; Li, H.; Gong, Y.; Zhu, K.; Hu, X.-P.; Zhang, D.; Xu, Y.; Wang, Y.-Y.; He, K.; Ma, X.-C.; Zhang, S.-C.; Xue, Q.-K. Superconductivity in few-layer stanene. *Nat. Phys.* **2018,** *14* (4), 344-348, DOI: 10.1038/s41567-017-0031-6.

(9) Huang, B.; Clark, G.; Navarro-Moratalla, E.; Klein, D. R.; Cheng, R.; Seyler, K. L.; Zhong, D.; Schmidgall, E.; McGuire, M. A.; Cobden, D. H.; Yao, W.; Xiao, D.; Jarillo-Herrero, P.; Xu, X. Layer-dependent ferromagnetism in a van der Waals crystal down to the monolayer limit. *Nature* **2017,** *546* (7657), 270-85, DOI: 10.1038/nature22391.

View Article Online
DOI: 10.1039/D0NR04837B

(10) Neto, A. C.; Guinea, F.; Peres, N. M.; Novoselov, K. S.; Geim, A. K. The electronic properties of graphene. *Rev. Mod. Phys.* **2009,** *81* (1), 109.

(11) Guan, Z.; Ni, S. Insights from first principles graphene/g-C2N bilayer: gap opening, enhanced visible light response and electrical field tuning band structure. *Appl. Phys. A* **2017,** *123* (11), 678, DOI: 10.1007/s00339-017-1314-6.

(12) Guan, Z.; Lian, C.-S.; Hu, S.; Ni, S.; Li, J.; Duan, W. Tunable Structural, Electronic, and Optical Properties of Layered Two-Dimensional C2N and MoS2 van der Waals Heterostructure as Photovoltaic Material. *J. Phys. Chem. C* **2017,** *121* (6), 3654-3660, DOI: 10.1021/acs.jpcc.6b12681.

(13) Wolf, S. A.; Awschalom, D. D.; Buhrman, R. A.; Daughton, J. M.; von Molnar, S.; Roukes, M. L.; Chtchelkanova, A. Y.; Treger, D. M. Spintronics: A spin-based electronics vision for the future. *Science* **2001,** *294* (5546), 1488-1495, DOI: 10.1126/science.1065389.

(14) Guan, Z.; Wang, J.; Huang, J.; Wu, X.; Li, Q.; Yang, J. Metal-Free Magnetism and Half-Metallicity of Carbon Nitride Nanotubes: A First-Principles Study. *J. Phys. Chem. C* **2014,** *118* (39), 22491-22498, DOI: 10.1021/jp508617k.

(15) Guan, Z.; Si, C.; Hu, S.; Duan, W. First-principles study of line-defect-embedded zigzag graphene nanoribbons: electronic and magnetic properties. *Phys. Chem. Chem. Phys.* **2016,** *18* (17), 12350-12356, DOI: 10.1039/C6CP01263A.

(16) Mermin, N. D.; Wagner, H. Absence of Ferromagnetism or Antiferromagnetism in One- or Two-Dimensional Isotropic Heisenberg Models. *Phys. Rev. Lett.* **1966,** *17* (22), 1133-1136, DOI: 10.1103/PhysRevLett.17.1133.

(17) Deng, Y.; Yu, Y.; Song, Y.; Zhang, J.; Wang, N. Z.; Sun, Z.; Yi, Y.; Wu, Y. Z.; Wu, S.; Zhu, J.; Wang, J.; Chen, X. H.; Zhang, Y. Gate-tunable room-temperature ferromagnetism in two-dimensional Fe_3GeTe_2. *Nature* **2018,** *563* (7729), 94-+, DOI: 10.1038/s41586-018-0626-9.

(18) Žutić, I.; Fabian, J.; Das Sarma, S. Spintronics: Fundamentals and applications. *Rev. Mod. Phys.* **2004,** *76* (2), 323-410, DOI: 10.1103/RevModPhys.76.323.

(19) Huang, B.; Cenker, J.; Zhang, X.; Ray, E. L.; Song, T.; Taniguchi, T.; Watanabe, K.; McGuire, M. A.; Xiao, D.; Xu, X. Tuning inelastic light scattering via symmetry control

View Article Online
DOI: 10.1039/D0NR04837B

in the two-dimensional magnet CrI_3. *Nat. Nanotech.* **2020,** *15*, DOI: 10.1038/s41565-019-0598-4.

(20) Sivadas, N.; Okamoto, S.; Xu, X.; Fennie, C. J.; Xiao, D. Stacking-Dependent Magnetism in Bilayer CrI3. *Nano Lett.* **2018,** *18* (12), 7658-7664, DOI: 10.1021/acs.nanolett.8b03321.

(21) Zhang, C.; Nie, Y.; Sanvito, S.; Du, A. First-Principles Prediction of a Room-Temperature Ferromagnetic Janus VSSe Monolayer with Piezoelectricity, Ferroelasticity, and Large Valley Polarization. *Nano Lett.* **2019,** *19* (2), 1366-1370, DOI: 10.1021/acs.nanolett.8b05050.

(22) Huang, C.; Du, Y.; Wu, H.; Xiang, H.; Deng, K.; Kan, E. Prediction of Intrinsic Ferromagnetic Ferroelectricity in a Transition-Metal Halide Monolayer. *Phys. Rev. Lett.* **2018,** *120* (14), 147601, DOI: 10.1103/PhysRevLett.120.147601.

(23) Gong, C.; Li, L.; Li, Z.; Ji, H.; Stern, A.; Xia, Y.; Cao, T.; Bao, W.; Wang, C.; Wang, Y.; Qiu, Z. Q.; Cava, R. J.; Louie, S. G.; Xia, J.; Zhang, X. Discovery of intrinsic ferromagnetism in two-dimensional van der Waals crystals. *Nature* **2017,** *546*, 265, DOI: 10.1038/nature22060.

(24) Yang, J.-H.; Xiang, H. Van der Waals engineering of magnetism. *Nat. Mater.* **2019,** *18*, 2, DOI: 10.1038/s41563-019-0524-z.

(25) Bonilla, M.; Kolekar, S.; Ma, Y.; Diaz, H. C.; Kalappattil, V.; Das, R.; Eggers, T.; Gutierrez, H. R.; Manh-Huong, P.; Batzill, M. Strong room-temperature ferromagnetism in VSe_2 monolayers on van der Waals substrates. *Nat. Nanotech.* **2018,** *13* (4), 289-294, DOI: 10.1038/s41565-018-0063-9.

(26) Wang, M.-C.; Huang, C.-C.; Cheung, C.-H.; Chen, C.-Y.; Tan, S. G.; Huang, T.-W.; Zhao, Y.; Zhao, Y.; Wu, G.; Feng, Y.-P.; Wu, H.-C.; Chang, C.-R. Prospects and Opportunities of 2D van der Waals Magnetic Systems. *Annalen der Physik*, 1900452, DOI: 10.1002/andp.201900452.

(27) Zheng, F.; Zhao, J.; Liu, Z.; Li, M.; Zhou, M.; Zhang, S.; Zhang, P. Tunable spin states in the two-dimensional magnet CrI3. *Nanoscale* **2018,** *10* (29), 14298-14303, DOI: 10.1039/C8NR03230K.

(28) Lee, I.; Utermohlen, F. G.; Weber, D.; Hwang, K.; Zhang, C.; van Tol, J.; Goldberger, J. E.; Trivedi, N.; Hammel, P. C. Fundamental Spin Interactions Underlying

View Article Online
DOI: 10.1039/D0NR04837B

the Magnetic Anisotropy in the Kitaev Ferromagnet CrI_3. *Phys. Rev. Lett.* **2020,** *124* (1), 017201, DOI: 10.1103/PhysRevLett.124.017201.

(29) Webster, L.; Yan, J.-A. Strain-tunable magnetic anisotropy in monolayer $CrCl_3$, $CrBr_3$, and CrI_3. *Phys. Rev. B* **2018,** *98* (14), 144411-8, DOI: 10.1103/PhysRevB.98.144411.

(30) Lu, A. Y.; Zhu, H.; Xiao, J.; Chuu, C. P.; Han, Y.; Chiu, M. H.; Cheng, C. C.; Yang, C. W.; Wei, K. H.; Yang, Y.; Wang, Y.; Sokaras, D.; Nordlund, D.; Yang, P.; Muller, D. A.; Chou, M. Y.; Zhang, X.; Li, L. J. Janus monolayers of transition metal dichalcogenides. *Nat Nanotechnol* **2017,** *12* (8), 744-749, DOI: 10.1038/nnano.2017.100.

(31) Li, R.; Cheng, Y.; Huang, W. Recent Progress of Janus 2D Transition Metal Chalcogenides: From Theory to Experiments. *Small* **2018,** *14* (45), 1802091, DOI: 10.1002/smll.201802091.

(32) Guan, Z.; Luo, N.; Ni, S.; Hu, S. Tunable Electronic and Magnetic Properties of Monolayer and Bilayer Janus Cr2Cl3I3: A First-Principles Study. *Materials Advances* **2020**, DOI: 10.1039/D0MA00085J.

(33) Peng, R.; Ma, Y.; Zhang, S.; Huang, B.; Dai, Y. Valley Polarization in Janus Single-Layer MoSSe via Magnetic Doping. *J. Phys. Chem. Lett.* **2018,** *9* (13), 3612-3617, DOI: 10.1021/acs.jpclett.8b01625.

(34) Dong, L.; Lou, J.; Shenoy, V. B. Large In-Plane and Vertical Piezoelectricity in Janus Transition Metal Dichalchogenides. *ACS Nano* **2017,** *11* (8), 8242-8248, DOI: 10.1021/acsnano.7b03313.

(35) Guo, Y.; Zhou, S.; Bai, Y.; Zhao, J. Enhanced piezoelectric effect in Janus group-III chalcogenide monolayers. *Appl. Phys. Lett.* **2017,** *110* (16), 163102, DOI: 10.1063/1.4981877.

(36) Chen, W.; Hou, X.; Shi, X.; Pan, H. Two-Dimensional Janus Transition Metal Oxides and Chalcogenides: Multifunctional Properties for Photocatalysts, Electronics, and Energy Conversion. *ACS Appl. Mater. Interfaces* **2018,** *10* (41), 35289-35295, DOI: 10.1021/acsami.8b13248.

(37) Guan, Z.; Ni, S.; Hu, S. Tunable Electronic and Optical Properties of Monolayer and Multilayer Janus MoSSe as a Photocatalyst for Solar Water Splitting: A

View Article Online
DOI: 10.1039/D0NR04837B

First-Principles Study. *J. Phys. Chem. C* **2018,** *122* (11), 6209-6216, DOI: 10.1021/acs.jpcc.8b00257.

(38) Xu, C.; Feng, J.; Prokhorenko, S.; Nahas, Y.; Xiang, H.; Bellaiche, L. Topological spin texture in Janus monolayers of the chromium trihalides $Cr(I,X)_3$. *Phys. Rev. B* **2020,** *101* (6), 060404, DOI: 10.1103/PhysRevB.101.060404.

(39) Liu, Y.; Huang, Y.; Duan, X. Van der Waals integration before and beyond two-dimensional materials. *Nature* **2019,** *567* (7748), 323-333, DOI: 10.1038/s41586-019-1013-x.

(40) Jiang, S.; Shan, J.; Mak, K. F. Electric-field switching of two-dimensional van der Waals magnets. *Nat. Mater.* **2018,** *17* (5), 406-411, DOI: 10.1038/s41563-018-0040-6.

(41) Burch, K. S. Electric switching of magnetism in 2D. *Nat. Nanotech.* **2018,** *13* (7), 532-532, DOI: 10.1038/s41565-018-0165-4.

(42) Sun, Z.; Yi, Y.; Song, T.; Clark, G.; Huang, B.; Shan, Y.; Wu, S.; Huang, D.; Gao, C.; Chen, Z.; McGuire, M.; Cao, T.; Xiao, D.; Liu, W.-T.; Yao, W.; Xu, X.; Wu, S. Giant nonreciprocal second-harmonic generation from antiferromagnetic bilayer CrI3. *Nature* **2019,** *572* (7770), 497-501, DOI: 10.1038/s41586-019-1445-3.

(43) Gibertini, M.; Koperski, M.; Morpurgo, A. F.; Novoselov, K. S. Magnetic 2D materials and heterostructures. *Nat. Nanotech.* **2019,** *14* (5), 408-419, DOI: 10.1038/s41565-019-0438-6.

(44) Ma, Y.; Dai, Y.; Guo, M.; Niu, C.; Zhu, Y.; Huang, B. Evidence of the Existence of Magnetism in Pristine VX_2 Monolayers (X = S, Se) and Their Strain-Induced Tunable Magnetic Properties. *ACS Nano* **2012,** *6* (2), 1695-1701, DOI: 10.1021/nn204667z.

(45) Cheng, Y. C.; Zhu, Z. Y.; Tahir, M.; Schwingenschlögl, U. Spin-orbit–induced spin splittings in polar transition metal dichalcogenide monolayers. *EPL (Europhysics Letters)* **2013,** *102* (5), 57001, DOI: 10.1209/0295-5075/102/57001.

(46) Jian, P.; Li, L.; Liao, Z.; Zhao, Y. X.; Zhong, Z. Spin Direction-Controlled Electronic Band Structure in Two-Dimensional Ferromagnetic CrI3. *Nano Lett.* **2018,** *18* (6), 3844-3849, DOI: 10.1021/acs.nanolett.8b01125.

(47) Wang, Y.; Lv, J.; Zhu, L.; Ma, Y. Crystal structure prediction via particle-swarm optimization. *Phys. Rev. B* **2010,** *82* (9), 094116, DOI: 10.1103/PhysRevB.82.094116.

View Article Online
DOI: 10.1039/D0NR04837B

(48) Kresse, G.; Furthmüller, J. Efficient iterative schemes for ab initio total-energy calculations using a plane-wave basis set. *Phys. Rev. B* **1996,** *54* (16), 11169-11186, DOI: 10.1103/PhysRevB.54.11169.

(49) Kresse, G.; Furthmuller, J. Efficiency of ab-initio total energy calculations for metals and semiconductors using a plane-wave basis set. *Comp. Mater. Sci.* **1996,** *6* (1), 15-50, DOI: Doi 10.1016/0927-0256(96)00008-0.

(50) Perdew, J. P.; Burke, K.; Ernzerhof, M. Generalized Gradient Approximation Made Simple. *Phys. Rev. Lett.* **1996,** *77* (18), 3865-3868, DOI: 10.1103/PhysRevLett.77.3865.

(51) Liechtenstein, A. I.; Anisimov, V. I.; Zaanen, J. Density-functional theory and strong interactions: Orbital ordering in Mott-Hubbard insulators. *Phys. Rev. B* **1995,** *52* (8), R5467-R5470, DOI: 10.1103/PhysRevB.52.R5467.

(52) Heyd, J.; Scuseria, G. E.; Ernzerhof, M. Hybrid functionals based on a screened Coulomb potential. *J. Chem. Phy.* **2003,** *118* (18), 8207-8215, DOI: 10.1063/1.1564060.

(53) Heyd, J.; Scuseria, G. E.; Ernzerhof, M. Erratum: “Hybrid functionals based on a screened Coulomb potential” [J. Chem. Phys. 118, 8207 (2003)]. *J. Chem. Phy.* **2006,** *124* (21), 219906, DOI: 10.1063/1.2204597.

(54) Monkhorst, H. J.; Pack, J. D. Special points for Brillouin-zone integrations. *Phys. Rev. B* **1976,** *13* (12), 5188-5192, DOI: 10.1103/PhysRevB.13.5188.

(55) Togo, A.; Tanaka, I. First principles phonon calculations in materials science. *Scripta Mater.* **2015,** *108*, 1-5.

(56) Nosé, S. A unified formulation of the constant temperature molecular dynamics methods. *J. Chem. Phy.* **1984,** *81* (1), 511-519, DOI: 10.1063/1.447334.

(57) Srivastava, A.; Sidler, M.; Allain, A. V.; Lembke, D. S.; Kis, A.; Imamoğlu, A. Optically active quantum dots in monolayer WSe2. *Nat. Nanotech.* **2015,** *10* (6), 491-496, DOI: 10.1038/nnano.2015.60.

(58) Aivazian, G.; Gong, Z.; Jones, A. M.; Chu, R.-L.; Yan, J.; Mandrus, D. G.; Zhang, C.; Cobden, D.; Yao, W.; Xu, X. Magnetic control of valley pseudospin in monolayer WSe_2. *Nat. Phys.* **2015,** *11* (2), 148-152, DOI: 10.1038/nphys3201.

(59) Lee, J.; Mak, K. F.; Shan, J. Electrical control of the valley Hall effect in bilayer MoS2 transistors. *Nat. Nanotech.* **2016,** *11* (5), 421-425, DOI: 10.1038/nnano.2015.337.

View Article Online
DOI: 10.1039/D0NR04837B

(60) Schaibley, J. R.; Yu, H.; Clark, G.; Rivera, P.; Ross, J. S.; Seyler, K. L.; Yao, W.; Xu, X. Valleytronics in 2D materials. *Nat. Rev. Mater.* **2016,** *1* (11), 16055, DOI: 10.1038/natrevmats.2016.55.

(61) Xiang, H. J.; Wei, S.-H.; Whangbo, M. H. Origin of the Structural and Magnetic Anomalies of the Layered Compound $SrFeO_2$: A Density Functional Investigation. *Physical Review Letters* **2008,** *100* (16), 167207, DOI: 10.1103/PhysRevLett.100.167207.

(62) Pick, Š.; Dreyssé, H. Magnetic anisotropy of transition-metal thin films. *Phys. Rev. B* **1993,** *48* (18), 13588-13595, DOI: 10.1103/PhysRevB.48.13588.

(63) Wang, D.-s.; Wu, R.; Freeman, A. J. First-principles theory of surface magnetocrystalline anisotropy and the diatomic-pair model. *Phys. Rev. B* **1993,** *47* (22), 14932-14947, DOI: 10.1103/PhysRevB.47.14932.

View Article Online
DOI: 10.1039/D0NR04837B

TOC